Fabrication on porous alumina tube by centrifugal molding

Chun-Hong Chen[*], Kanji Takita, Satoshi Ishiguro, Sawao Honda, Hideo Awaji

Department of Materials Science and Engineering, Nagoya Institute of Technology, Gokiso-cho, Showa-ku, Nagoya 466 8555, Japan

Abstract

The material design model for porous materials is proposed. Porous alumina tubes are fabricated by using two different α-alumina powders with narrow size distribution (AES-12 and TM-D) by centrifugal molding technique. The experimental results show TM-D is limited to get the homogenous structure and AES-12 offers a good flexibility in gradient design, which depends on the slurry character. The bimodal pore structure of the tubes is constructed from large spherical pores about 10 μm formed by PMMA particles and small sub-micrometer pores which are the results of the lower packing density in centrifugal process and the lower sintering temperature. The ratio of the macro spherical pore to sub-micrometer pore varies with the amount of PMMA particles, and hence the bimodal pore structure of porous tubes is very useful to control the air permeability. The fracture strength of O-ring increases with the decrease in porosity regardless of the pore gradient of the tubes. The pore-graded tubes show the higher strength than homogenous tubes while keeping the same porosity in the inner wall.
© 2004 Elsevier Ltd. All rights reserved.

Keywords: Centrifugal molding; Porous alumina; Porosity gradients; Fracture strength; Al_2O_3 Permeability

1. Introduction

Porous ceramics are used as gas/liquid separators, catalyst supports and molecular sieves which can be used at high temperature and under severe chemical conditions. There are several approaches for the fabrication of micro/macro porous ceramics in recent times, which can be mainly divided into the following four groups.[1] (1) Controlling the particle size of ceramics to maintain constant pores among particles. (2) Reducing the forming pressure and/or sintering temperature. (3) Mixing the ceramic powders with a bubble former so that large and homogenous pores can be introduced. (4) Mixing ceramic powders with additional organic particles, which vaporize at relatively low temperatures and form small and homogenous pores. A sol–gel process with the presence of a surfactant has been developed to prepare mesoporous ceramics with a well-ordered arrangement of pores.[2] Recently porous ceramics have been developed with high-temperature stability, strength, catalytic activity, erosion resistance and corrosion resistance. In spite of these excellent properties, the potential of porous ceramics has not been fully realized because of their well-known problems, such as lack of pore size control, lack of continuous processing method, and absence of a model relating pore structure to mechanical properties.

In a Functionally Graded Material (FGM), the composition and structure gradually change over volume, resulting in corresponding changes in the properties of the material. The most familiar FGM is compositionally graded from a refractory ceramic to a metal. It can incorporate incompatible functions such as the heat, wear, and oxidation resistance of ceramics and the high toughness, machinability and bonding capability of metals. In recent years, the FGM concept is introduced for the porous materials, where pores are the important structural ingredients for FGMs. The design of FGMs is now focused on the optimization of its structure to yield appropriate residual stress and minimize the thermal stresses, which would simulate the in-service and the thermal

* Corresponding author. Tel.: +81 52 735 5276; fax: +81 52 735 5276.
E-mail address: chunhong@zymail.mse.nitech.ac.jp (C.-H. Chen).

shock environment of FGM cylinders.[3–6] Centrifugal molding is an economical and convenient method to fabricate a hollow cylinder. Hollow cylinders with a functional gradient were also fabricated using the centrifugal molding technique with the difference in the centrifugal force between powder mixtures to create a compositional gradient along the radial direction due to the difference in their densities and particle sizes.[7,8] The gradient of the tubes varying from an homogenous structure to a bilayered structure can be controlled by adjusting the slurry character.[9] In this paper, the fabrication of porous alumina tubes produced by the centrifugal molding and some contents and ideas underlying in the design of porous materials were described. Cylindrical porous ceramic tubes were fabricated in the presence of an organic pore forming agent. Two kinds of commercial α-alumina were used to examine the possibility for porous tubes with gradient and homogeneous structures.

2. Concept of material design

Global understanding of the relations among chemical composition, crystal structure and properties of materials on the basis of a suitable classification is a root concept of material design. To design new materials, it is required to search for the best solution for the in-service environment's needs that are controlled by many parameters. In general, it is impossible to search all possibilities by experiment.

A material design scheme for porous materials applicable to high temperature environment is shown in Fig. 1. Alumina is used as material for the high temperature environment, since it has acceptable physical properties, including good thermal conductivity, refractoriness, and chemical durability. Materials for the filter require a particular mean size, porosity to keep the balance between the high strength and good permeability.[10] It is attempted for the outer part to act as the support, which should be mechanically strong and offers good permeability and the inner part as the separation medium due to the pore gradient of the cylinder.[11] These material attributes must be coupled to an appropriate thermal design so that the filter can survive extreme temperature gradients generated during the regeneration process. The high
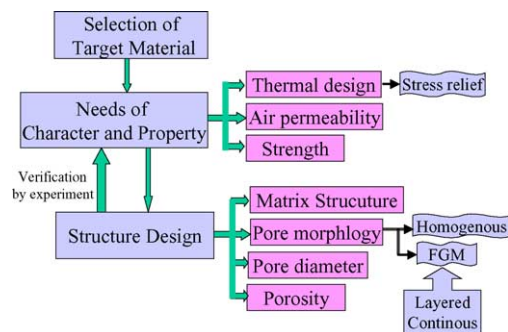
thermal shock resistance of porous materials is due to the infiltration effect of cooling media.[12] The property that is most directly related to the design of a structure of filter is the void space through which fluid flows. The pore morphology can be divided into the homogenous structure and FGM, which is composed of layered and continuous gradient. It is easy to control the pore gradient of the tube using the laminated method of the centrifugal molding technique.[13] Whenever two laminate are present, the interface problems such as lamination/stress concentration appeared which depends on the compositional changes of the matrix materials.[14,15] Finally, the results from the design model should be verified to satisfy the desired properties in considering applications of the filter.

3. Experimental procedure

3.1. The starting materials

The two different α-alumina powders used in this study were TM-D (Taimei Chemical Co., Ltd.) and AES-12 (Sumitomo Chemical Co., Ltd.) with a BET surface of 11.4 and $6 \, m^2/g$, respectively. Both alumina powders have a narrow particle size distributions with a mean particle size of 0.25 and 0.5 μm, respectively. Polymethylmethacrylate (PMMA) powder with an average particle size of 10 μm was used as pore forming agent. PMMA particles are the desirable pore forming agent for macropores due to their homogenous particle sizes and low vaporization temperature.[10] For good dispersion, Dispersant DarvanC and Seruna D-305 were added to TM-D and AES-12, respectively, along with distilled water as solvent. 0.25 mass% of MgO was added as the sintering aid and grain growth inhibitor.

3.2. Processing

The alumina powders and PMMA particles were first mixed with the dispersant by magnetic stirring for 1 h. The mixed slurry was treated ultrasonically to break down particle agglomerates. Finally, the slurry was deaired in vacuum for 15 min and poured in the stainless steel mold of dimension in the inner diameter of 20 mm and the length of 70 mm.

For easy removal of the sample after drying, the inner surface of the mold was pre-coated with vaseline as a lubricant. The cylindrical mold was centrifuged around the radial axis with a speed of 3000 rpm for 15 min. The residual liquid was poured out after centrifugation. The finished green tubes were dried vertically inside the mold itself by keeping it in the vacuum chamber so that the shape was maintained. The temperature was allowed to rise to 100 °C with a ramp of 10 °C/h. The tubes shrunk and released easily from the mold during drying. The PMMA was dissociated completely by heating at 500 °C for 1 h with a controlled heating rate of 30 °C/h. The green tubes after calcination were sintered at 1350 °C for 1 h in air atmosphere.
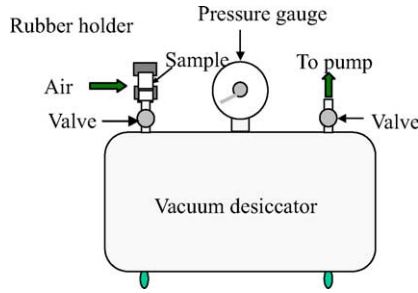

Fig. 1. The concept of material design for porous materials.

Fig. 2. Schematic diagram of air permeability measuring equipment.

3.3. Characterization

The density and porosity of sintered tubes was measured by Archimedes method with distilled water as media. Microstructures of the sintered specimen were examined by Scanning Electron Microscope (SEM) on the cross-sectional surfaces in equal intervals along the radius.

Both ends of the tube were covered with polymer end caps and one of the ends of tube was connected to the vacuum desiccator shown as Fig. 2. The time for a pressure decrease from 0.005 to 0.01 MPa was measured. The air permeability of the tube along the radial direction can be calculated as follows:[16]

$$K = \frac{lQ}{A\Delta P} \tag{1}$$

where K (cm²/s MPa) is the air permeability, l (cm) is the thickness of the tube, Q (cm³/s) is the rate of air flow, A is the cross-section, and ΔP is the pressure decrement.

For mechanical evaluation, the tubes were cut into 5 mm in length by a diamond cutter and subjected to ring diametral compression testing using a mechanical testing machine (Instron 5582, Japan) with a crosshead speed of 0.5 mm/min. The fracture strength of the tubes with a homogenous structure was determined using the following equation:[17]

$$F = 0.9555 \frac{P(D-d)}{Bd^2} \tag{2}$$

The fracture strength of the tubes with the pore gradient can be estimated based on the curved beam theory.[13] The schematic representation of the O-ring compression testing is shown in the Fig. 3 (1/4 O-ring). The stress distribution of graded ring specimen with a rectangular cross-section, the hoop stress σ_θ are expressed as following:

$$\sigma_\theta = E(x) \frac{\varepsilon_0 \rho + y\omega}{\rho + y} \tag{3}$$

where ε_0 is a strain at a centroid, ρ is the radius of the center axis, y is the layer distance from the centerline and ω is the angular strain, x is the non-dimensional distance along the radial direction and $E(x)$ is the radial gradient of Young's modulus. The axial load N and the moment M at any radial plane of angle φ are balanced with the applied load P and are
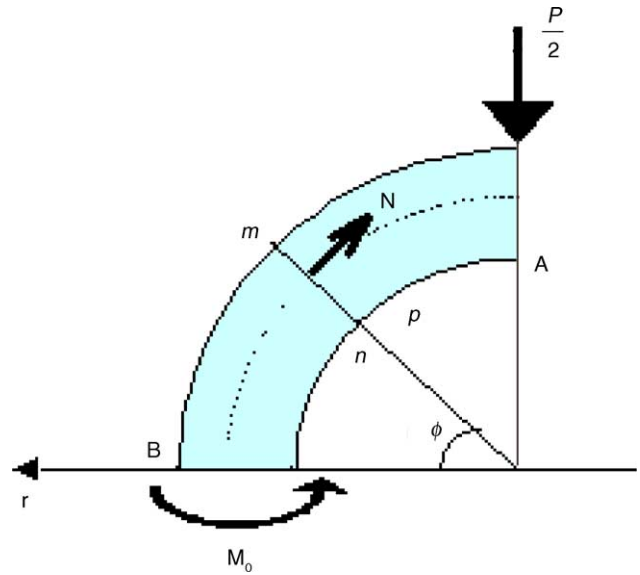

Fig. 3. Schematic illustration of the diametral compression testing.

given by the following equations:

$$N = -\frac{P}{2}\cos\phi = \int_A \sigma_\theta \, dA \tag{4}$$

$$M = M_0 - \frac{P\rho}{2}(1-\cos\phi) = \int_A \sigma_\theta y \, dA \tag{5}$$

where A is the area of the cross-section, M_0 is a statically indeterminate moment working on the cross-section m–n to prevent the rotation together with the axial load and can be calculated referring to the Castigliano's First Theorem.

The analysis shows that the maximum stress is applied to the inside of the ring along the load axis and can be regarded as the fracture strength of the ring based on the maximum hoop stress.

4. Results and discussion

4.1. Microstructure

The porous tubes prepared are shown in Fig. 4, where no any defects, like delamination or crack are observed after sintering. The specimens made from AES-12 and TM-D are denoted as SA and ST, respectively. In the case of ST samples, the experimental results show the slurry character certainly varies with the solid load and dispersant concentration of the slurry as expected. However, the perfect tubes without any delamination and cracks are not obtained during the centrifugal molding except that the dispersant concentration is kept at 0.07 wt.% and the solid load is 37 vol.%.

A composed SEM micrograph of the cross-section of specimens with the presence of 30 vol.% PMMA particles is shown in Fig. 5. Pores appear as black areas. The structure is same from the inner wall to outer wall of the tube and

Fig. 4. The porous tube specimen.

spherical pores distribute uniformly in the alumina matrix. This is due to the narrow particle size distribution in TM-D and the solid load in the slurry is high.

Fig. 6 shows the microstructures of ST samples with 0%, 10% and 50% PMMA additions by volume. Grain growth of alumina particles is not observed and continuous but sub-micrometer pores exist among the alumina grains (Fig. 6A). On the addition of the pore-forming agent
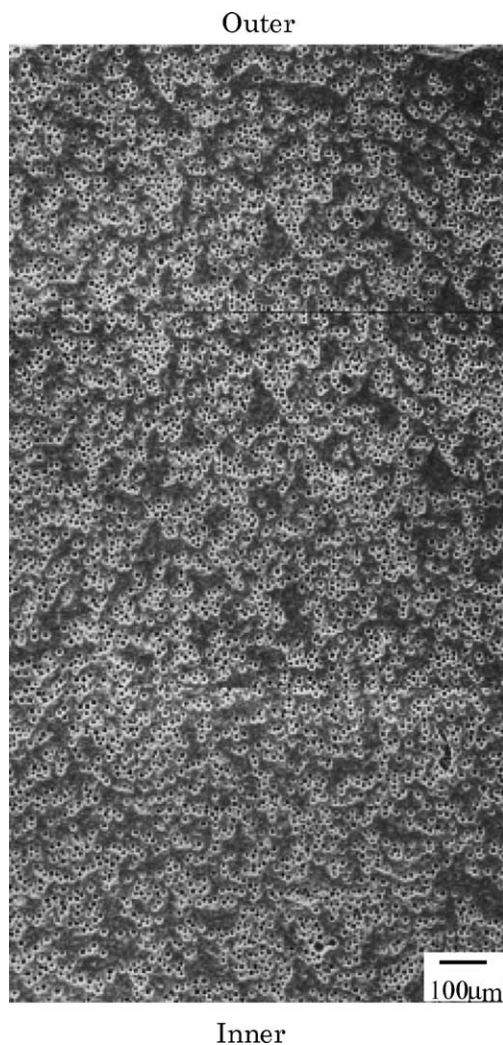

Fig. 5. Continuous SEM photograph for ST with 30 vol.% PMMA.
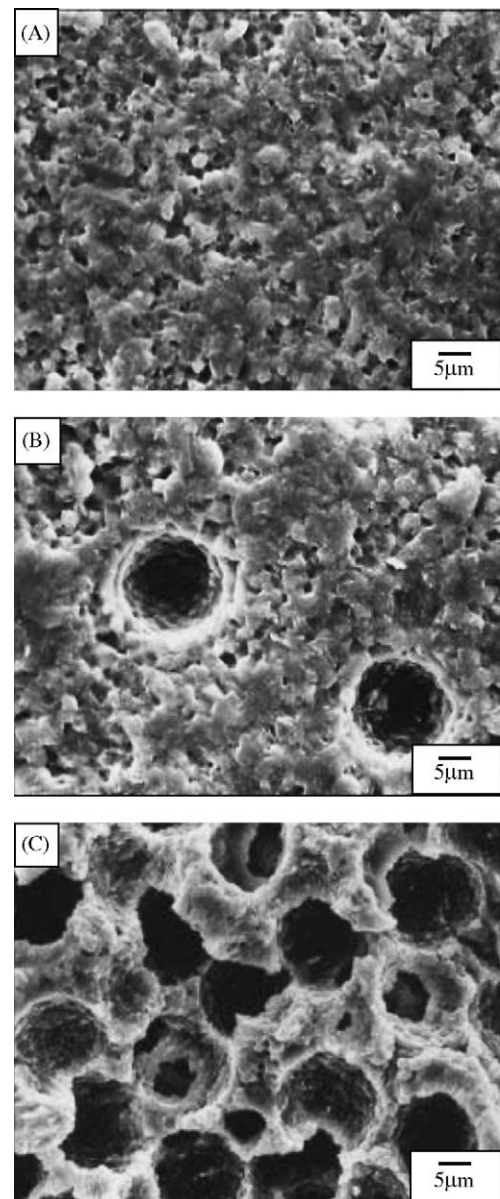

Fig. 6. SEM photographs for ST samples: (A) without PMMA, (B) with 10 vol.% PMMA, and (C) with 50 vol.% PMMA.

PMMA, spherical pores with 10 μm in diameter could be clearly observed. The isolated spherical pores are connected with a sub-micrometer pore (10 vol.% PMMA). The spherical pores were observed uniformly in the alumina matrix to form a three-dimensional network and also to serve as open pore regardless of the sub-micrometer porosity (50 vol.% PMMA). It is also clear that the size of sub-micrometer pores varies with the PMMA amount owning to the different packing structure. A similar pattern in the bimodal pore structure with different amounts of PMMA is revealed for the SA specimen as well. However, the sub-micrometer pores in SA samples mainly result from the partial sintering. It is also found the difficulty in the preparation of the SA samples with the presence of PMMA amount above 30 vol.%.

All slurries made from the AES-12 powder are prepared when the minimum in liquid volume is used to keep the specimen SA form. Fig. 7 shows the microstructure of the specimen with no dispersant and 0.2 wt.% dispersant in the absence of PMMA particles. No difference in microstructures from the inner wall to outer wall of the tube is observed though the dispersant concentration varies. Sub-micrometer pores existed among alumina grains are almost channelled with well-known necks. This is due to the sintering mechanisms without complete densification.
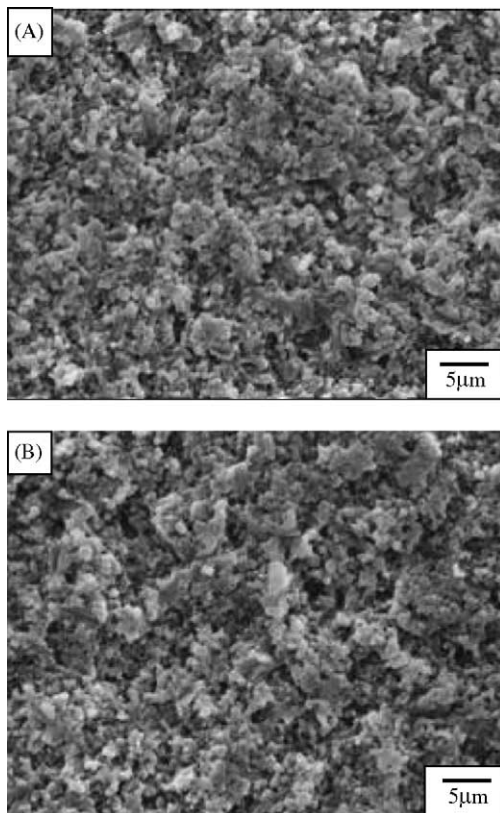

Fig. 7. SEM photographs for SA samples: (A) without dispersant and (B) with 0.2 wt.% dispersant.
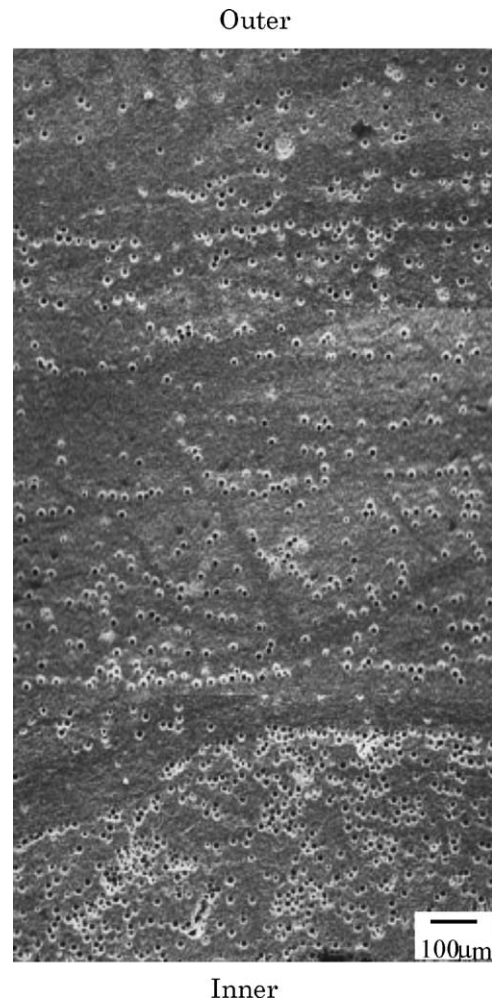

Fig. 8. Continuous SEM photograph for continuous graded SA samples with 10 vol.% PMMA.

A composed SEM microstructure of 10 vol.% PMMA graded tubes of SA samples is shown in Fig. 8, where the dispersant concentration is kept at 0.05 wt.%. The distribution of spherical pores is graded along the radial direction owning to the difference in centrifugal force on the alumina and PMMA particles. To observe the distribution of spherical pore in quantity, the square cross-section is divided into 10 level sections, and the number of pores is counted within each small areas (100 μm × 100 μm) in equal intervals of distance along the radial direction. Fig. 9 shows the number of pores measured decreases from inner wall towards outer wall of the tube. For the specimen of 20 vol.% PMMA, there is a continuous decrease along the radius. For the specimen with 30 vol.% PMMA, a minimum in pore density is observed. This phenomenon is due to difference in the network formation process by particle settling in the slurry, where the formation mechanism is essentially attributed to collisions of dispersed particles and hence the difference in their settling velocities under centrifugal field.[18,19] The experimental results show the pore density along the radial direction can be
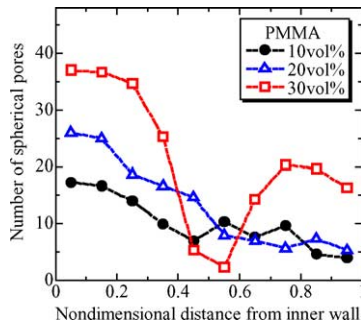
Fig. 9. Pore distribution for continuous graded SA samples.

changed by selecting dispersant concentration and the solid load in the slurry.

4.2. Porosity

The porosity of the sample varies with the volume fraction of PMMA as shown in Fig. 10, where no dispersant is used in the slurry. As expected, the porosity increases linearly with the increase of PMMA amount. The ST sample yields a porosity of approximately 5% even without PMMA particles, probably because the sub-micrometer pores exist owning to the lower packing density in centrifugal process. For the SA samples, a higher porosity results with the presence of the same PMMA content. This expected because the lower sintering temperature does not remove the many sub-micrometer pores in the alumina matrix, as observed in Fig. 7.

The relationship between the amount of PMMA and open porosity is shown in Fig. 11, where no dispersant is used in the slurry of SA. The open porosity of ST increases linearly when PMMA amount is kept below 35 vol.%, and is jumped suddenly up to 90 vol.% with addition of more PMMA because the spherical pores are connected with the sub-micrometer pores. Since almost all pores appear as open pores in SA samples, the porosity is constant at about 95%. Fig. 12 shows the effect of dispersant concentration on the porosity of the SA samples. The porosity decreases with increase in dispersant concentration. However, when PMMA is added with 30 vol.%, the lowest porosity (about 17%) is shown with the addition of 1 wt.% dispersant. The discrepancy suggests
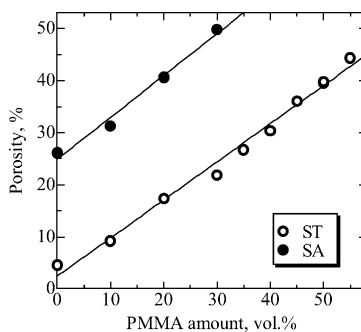
that the slurry is unstable and hence a bilayered structure is formed, the PMMA layer lying in the inner wall vaporizes after sintering. It is also visible that the porosity is lower than without PMMA particles. This is probably because the good fluidity of the slurry densifies the alumina matrix better.

The influence of the solid load on the porosity of SA samples is shown in Fig. 13 by keeping the volume fraction of PMMA at 10 vol.%. As is obvious from the figure, the porosity increases with increasing solid load, and varies with the dispersant concentration at constant solid load. Possibly, an increase in dispersant concentration and a decrease in the solid load lower the viscosity and raise the fluidity of the slurry. These results show that the slurry character is the essential factor and that within a wide range it is possible to control the porosity of the tube with the use of AES-12.
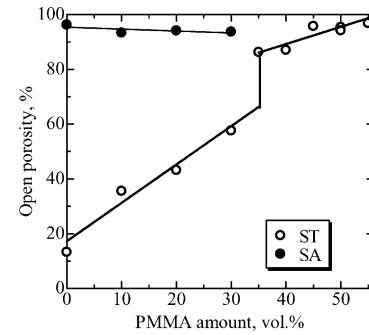

Fig. 11. Relationship between PMMA amount and open porosity for SA and ST samples.
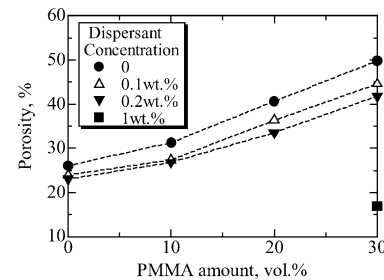
Fig. 12. The effect of dispersant concentration on the porosity for ST samples.

Fig. 10. Relationship between PMMA amount and porosity for SA and ST samples.

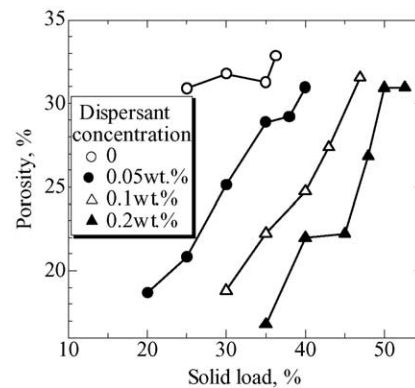Fig. 13. The effect of solid load on the porosity for ST samples.

Fig. 14. Relationship between open porosity and air permeability for SA and ST samples.
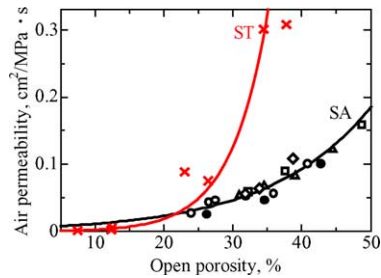

Fig. 15. Relationship between open porosity and fracture strength for SA and ST samples.

4.3. Air permeability

The effect of open porosity on the air permeability of ST and SA samples is shown in Fig. 14, where $\triangle$, $\square$, $\diamondsuit$ indicate the air permeability of laminated samples (2 layers, 3 layers, 4 layers) of SA[11] and $\bigcirc$ land $\bullet$ indicate the homogeneous and continuous graded types, respectively. The experimental results show that the air permeability is independent of the pore distribution along the radial direction of the tubes if the open porosity is kept same as in the SA sample. There is a continuous gradual increase of the air permeability with increasing open porosity in the SA samples, but this is not true for the ST samples. The reason for the sharp increase of air permeability in ST samples (with an open porosity $\approx$30%) is due to the difference in the principle route for air transport from the sub-micrometer pore network to the spherical pore network, which can be clearly seen in the micrograph. The spherical pores are almost with well-grown necks and are lower in friction of fluid flow than those with irregular sub-micrometer pores. Therefore, porous materials with more spherical pores have higher air permeability than those with sub-micrometer pores. This is why the air permeability of ST samples is higher than that of SA samples. It is expected that the presence of the sharp increase of air permeability after solving the problem on the preparation of SA samples with more addition of PMMA particles. The results show the ratio of the macro spherical pore to sub-micrometer pore varies with the amount of PMMA particles, and hence the bimodal pore structures of porous tubes are very useful to control the air permeability.

4.4. Fracture strength

The effect of porosity of the inner wall on the fracture strength (the average value) is shown in Fig. 15. The fracture strength increases with decreasing porosity in the ST and SA samples regardless of the pore distribution. The strength of the SA samples is little lower than that of ST samples when the porosity is greater than about 25%. This may be because of the loose packing in alumina matrix in SA samples without complete densification. The relationship between mechanical strength and the microstructure of the tube should be studied fu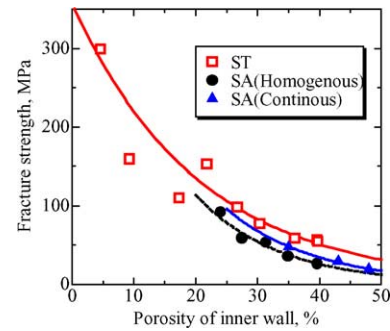rther. The SA sample with continuous pore gradient shows higher strength than that with homogeneous structure at the same porosity of the inner wall. This is because there are fewer pores on the outer wall by the pore gradient. A considerable dispersion of fracture strength is visible in the region of low porosity for the ST samples. The reasons could be that fracture origin is randomly changed from the sub-micrometer pores to the spherical pores.

5. Conclusions

A design model for porous materials is proposed. Porous alumina tubes are fabricated using two different alumina powders with narrow size distribution (AES-12 and TM-D) by centrifugal molding. The experimental results show that the TM-D powder is limited to obtain the homogeneous structures and the AES-12 powder offers a good flexibility in gradient design, dependent on the slurry character. The bimodal pore structure exists in the porous tubes, where submicrometer pores are introduced by the lower packing density in the centrifugal process and by the lower sintering temperature (only AES-12), while spherical pores about $10 \, \mu$m are formed with the evaporation of PMMA particles. The air permeability increases with the increase of the porosity, and can be controlled by the bimodal pore distribution. The fracture strength of O-rings increases with decreasing porosity regardless of the pore distribution of the tubes. The SA samples with continuous pore gradient show higher strength than those with homogenous structure at the same porosity of the inner wall.

References

1. Ishizaki, K., Komarneni, S. and Nanko, M., *Porous Materials— Process Technology and Applications*. Kluwer Academic Publishers, The Netherlands, 1998 (Chapter 2).
2. Beck, J. S., Vartuli, J. C., Loth, W. J., Leonowich, M. E., Lson, D. H., Sheppard, E. W. *et al.*, *J. Am. Chem. Soc.*, 1992, **114**, 10834–10843.
3. Markworth, A. J. and Saunders, J. H., A model of structure optimization for a functionally graded material. *Mater. Lett.*, 1995, **22**, 103–107.
4. Awaji, H. and Sivakumar, R., Temperature and stress distributions in a hollow cylinder of fucntionally graded material: the case of

temperature-independent material properties. *J. Am. Ceram. Soc.*, 2001, **84**(5), 1056–1065.

5. Tanigawa, Y., Oka, N., Akai, T. and Kawamura, R., One-dimensional transient thermal stress problem for nonhomogenous hollow circular cylinder and its optimization of material composition for thermal stress relaxation. *JSME Int. J. Ser. I*, 1997, **40A**(2), 117–127.

6. Tanigawa, Y., Some basic thermoelastic problems of nonhomogeneous structural materials. *Appl. Mech. Rev.*, 1995, **48**(6), 287–300.

7. Sivakumar, R., Nishikawa, T., Honda, S., Awaji, H. and Gnanam, F. D., Processing of mullite-molybdenum graded hollow cylinders by centrifugal molding technique. *J. Eur. Ceram. Soc.*, 2003, **23**(5), 765–772.

8. Sivakumar, R., Nishikawa, T., Honda, S. and Awaji, H., A novel technique applied for fabrication alumina/zirconia continuous graded hollow tubes. *J. Ceram. Soc. Jpn.*, 2002, **110**(5), 472–475.

9. Chen, C. H., Honda, S., Nishikawa, T. and Awaji, H., A hollow cylinder of functionally gradient materials fabricated by centrifugal molding technique. *J. Ceram. Soc. Jpn.*, 2003, **111**(7), 479–484.

10. Nishikawa, T., Nakashima, A., Honda, S. and Awaji, H., Effects of porosity and pore morphology and mechanical properties of porous alumina. *J. Soc., Mater. Sci., Jpn.*, 2001, **50**(6), 625–629.

11. Chao, W. J. and Chou, K. S., Studies on the control of porous properties in the fabrication of porous supports. *Key Eng. Mater.*, 1996, **115**, 93–108.

12. Tanaka, H., Maki, Y., Tsuboi, K., Honda, S., Nishikawa, T. and Awaji, H., Thermal stresses in porous materials under thermal shock by cooling medium-infiltration effect on thermal stress distributions. *J. Ceram. Soc. Jpn.*, 2004, **112**(3), 172–178.

13. Chen, C. H., Takita, K., Honda, S. and Awaji, H., Fracture behavior of cylindrical porous alumina with pore gradient. *J. Eur. Ceram. Soc.* (in press).

14. Chen, C. H., Awaji, H., Matsushima, Y., Kitaoka, S. and Nanjo, F., Analysis of temperature/stress distributions in a hot gas tubular ceramic filter under thermal shock. *J. Soc. Mater. Sci., Jpn.*, 2003, **52**(1), 63–68.

15. Jin, G. and Awaji, H., Residual thermal stresses in multilayered functionally graded material plates. *Mater. Sci. Res. Int.*, 2003, **9**(2), 125–130.

16. Kondo renyichi. *Porous materials—character and application, gihoudou, Japan*. 1973, p. 245.

17. Jadaan, O. M., Prediction of the strength of ceramic tubular components: Part I. Analysis. *J. Test Eval.*, 1991, **19**(3), 181–191.

18. Tsubaki, J., Mori, H., Kato, M., Okuda, K., Yoshida, Y. and Yokoyama, T., New slurry characterization Technique for optimizing wet-shaping process (Part 2). Dependency of centrifugal effect on slurry consolidation process. *J. Ceram. Soc. Jpn.*, 1998, **106**(6), 616–620.

19. Sugimoto, T., Mori, H. and Tsubaki, J., Network formation mechanism of fine particles in suspension-simulation on the structure formation in binary dispersions. *J. Soc. Powder Technol. Jpn.*, 2000, **37**, 100–106.